

QuantAttack: Exploiting Dynamic Quantization to Attack Vision Transformers

Amit Baras*, Alon Zolfi*, Yuval Elovici, Asaf Shabtai
Department of Software and Information Systems Engineering
Ben-Gurion University of the Negev, Israel

{barasa, zolfi}@post.bgu.ac.il, {elovici, shabtaia}@bgu.ac.il

Abstract

In recent years, there has been a significant trend in deep neural networks (DNNs), particularly transformer-based models, of developing ever-larger and more capable models. While they demonstrate state-of-the-art performance, their growing scale requires increased computational resources (e.g., GPUs with greater memory capacity). To address this problem, quantization techniques (i.e., low-bit-precision representation and matrix multiplication) have been proposed. Most quantization techniques employ a static strategy in which the model parameters are quantized, either during training or inference, without considering the test-time sample. In contrast, dynamic quantization techniques, which have become increasingly popular, adapt during inference based on the input provided, while maintaining full-precision performance. However, their dynamic behavior and average-case performance assumption makes them vulnerable to a novel threat vector – adversarial attacks that target the model’s efficiency and availability. In this paper, we present QuantAttack, a novel attack that targets the availability of quantized models, slowing down the inference, and increasing memory usage and energy consumption. We show that carefully crafted adversarial examples, which are designed to exhaust the resources of the operating system, can trigger worst-case performance. In our experiments, we demonstrate the effectiveness of our attack on vision transformers on a wide range of tasks, both uni-modal and multi-modal. We also examine the effect of different attack variants (e.g., a universal perturbation) and the transferability between different models.

1. Introduction

In recent years, deep neural networks (DNNs), particularly transformers [23], have made tremendous progress in various domains, such as NLP [21] and computer vision [22]. Their success stems mainly from their network size (which is ever increasing), which is based on the number of parameters they contain and the precision of the parameters (the

number of bits with which each parameter is represented). However, the high computational cost of their transformer blocks makes them unsuitable for many edge devices.

One way of reducing the size of the parameters is to quantize them to fewer bits and use low-bit-precision matrix multiplication. There are two types of quantization techniques: (a) quantization-aware training [2, 13, 47] - training a model with quantized parameters; and (b) post-training quantization [14, 30, 41] - quantizing parameters of a pre-trained model, which can be done in a static or dynamic (sample-dependent) manner. Recently, LLM.int8() [10], a dynamic post-training quantization technique, was proposed and integrated into Hugging Face [42], one of the largest open-source machine learning (ML) platforms. This technique decomposes the features and weights into sub-matrices of large magnitude features (outliers) and other values. The outlier feature matrices are multiplied in higher precision, while all other values are multiplied in lower precision, reducing inference time, memory usage, and energy consumption, without any degradation in performance. While LLM.int8() was originally proposed for the NLP domain, the application of quantization techniques extends to vision models, aiming to balance efficiency and performance while preserving crucial visual information for tasks like image classification and object detection. Despite the fact that quantization has been proven to be effective in making DNNs more resource-efficient, it also opens up a new attack surface for adversaries aiming to compromise model availability.

Given the potential impact of availability-oriented attacks, the ML research community has begun to direct its attention to adversarial attacks that target model availability. Shumailov *et al.* [36] were the first to present *sponge examples*, a technique that exploits data sparsity, causing the number of GPU operations to increase; this leads to increased inference time and energy consumption. Employing this attack vector, Cina *et al.* [6] poisoned models during the training phase to cause delays in the testing phase. Dynamic neural networks [17], which adapt their structures or parameters to the input during inference, have also been

*Equal contribution

shown to be susceptible to adversarial attacks. For example, adversarial attacks against models that employ early-exit strategies (a type of a dynamic network) have been studied extensively [18, 19, 31]. Research focusing on the post-processing phase of DNNs, particularly in object detection [35] and LiDAR detection [25], has shown that they are also susceptible to availability-oriented attacks.

In this paper, we introduce *QuantAttack*, a novel adversarial attack that specifically targets the quantization process and exploits its test-time dynamism in vision transformers. We argue that this attack vector poses a significant threat to the availability of transformer models due to the proposed attack’s broad generalizability to any type of network; this is due to the fact that the attack operates at the core level. Such attacks could have far-reaching implications, particularly in resource-constrained environments, where maintaining low latency and computational efficiency is paramount. To perform our attack, we employ the projected gradient descent (PGD) attack [26] and propose a custom loss function that aims to overload the matrix multiplication with high-bit precision (*i.e.*, outlier values) to trigger worst-case performance. To increase the stealthiness of our adversarial examples, we design our attack to preserve the model’s original classification. To assess the proposed attack’s effectiveness, in our evaluation, we perform experiments addressing: (i) modality - investigating uni-modal and multi-modal; (ii) model task - considering various computer vision applications; (iii) attack variations - single-image, class-universal, and universal; (iv) transferability - examining whether the perturbations are transferable between different models. Our experiments on the ViT model [12] show that the proposed attack can increase the model’s use of GPU memory by 23%, extend the GPU processing time by 11%, and expand energy use by 7%.

Our contributions can be summarized as follows:

- To the best of our knowledge, we are the first to both identify dynamic quantization as a novel threat vector and propose an adversarial attack that exploits the availability of quantized models.
- We design a stealthy attack that preserves the model’s original classification.
- We conduct a comprehensive evaluation on various configurations, examining different modalities and model tasks, reusable perturbations, transferability, and the use of ensembles.
- We present various countermeasures that can be employed to mitigate the threat posed by our attack.

2. Background & Related Work

2.1. Availability Attacks

Confidentiality, integrity, and availability, also known as the CIA triad, are a model that that typically serves as

the basis for the development of security systems [34]. In the context of DNNs, adversarial attacks targeting integrity [16, 28, 29, 37, 38, 45, 48, 49] and confidentiality [1, 20] have received a great deal of research attention over the last few years. However, adversarial attacks that target the availability of these models have only recently gained the attention of the ML research community. Shumailov *et al.* [36] were the pioneers in this area, introducing the sponge examples attack, a technique that primarily targets the efficiency of vision and NLP models. This approach exploits the data sparsity assumption that allows GPU acceleration and maximizes the number of GPU operations and memory accesses, which leads to an increase in the inference time. Employing the attack vector proposed in that work, Cina *et al.* [7] proposed sponge poisoning, a method aimed at degrading the performance of models by subjecting them to a sponge attack during the training phase. Further extending the applicability of the sponge attack, Boutros *et al.* [5] adapted the technique for FPGA devices, performing an adversarial attack that integrates malicious circuits to induce voltage drops, thereby generating timing faults in the targeted deep learning accelerators. Another noteworthy extension of the sponge was presented by Boucher [4] who introduced an adversarial attack on NLP models using invisible characters and homoglyphs, which, while undetectable to humans, can significantly alter the model’s output.

Dynamic neural networks [17], which optimize computational efficiency by adapting to input data during runtime, have also been shown to be vulnerable to adversarial attacks. Haque *et al.* [18] and Hong *et al.* [19] attacked DNNs that employ an early-exit strategy (dynamic depth), causing malicious inputs to always skip early exits, leading to worst-case performance. Pan *et al.* [31] proposed a unified formulation to construct adversarial samples to attack both the dynamic depth and width networks.

Another avenue of research, in which the post-processing phase of DNNs is targeted, has also been investigated. Shapira *et al.* [35] showed that overloading object detection models by increasing the total number of candidates input into the non-maximum suppression (NMS) component can lead to increased execution times. Liu [25] extended this to LiDAR detection models.

In this paper, we propose a novel attack vector that has not been studied before, an adversarial attack that targets the availability of dynamically quantized models.

2.2. Quantization

DNNs, particularly transformers, have achieved great success in various ML tasks [22, 43]. However, their computational complexity and large model size pose challenges for real-time applications and resource-limited devices. The size of a model is determined by the number of parameters

and their precision. The precision relates to the number of bits each weight value is stored with, typically 16 bits (also referred to as float16 or *f16*) or 8 bits (also referred to as int8 or *i8*). To mitigate these challenges, techniques like quantization are employed.

Quantization is used to reduce the computational time and memory consumption of neural networks. By quantizing the weights and activations into low-bit integers (*e.g.*, a 16-bit float to an 8-bit integer), GPU memory usage can be reduced and inference can be accelerated, due to low-bit-precision matrix multiplication. Two main quantization approaches have been proposed:

- **Quantization-Aware Training (QAT)**[2, 13, 47]: This method involves training the model with quantized weights and activations. QAT maintains good performance, even when using low-precision formats (*e.g.*, 2-bit format).
- **Post-Training Quantization (PTQ)**: This approach takes a pretrained model and quantizes it directly, eliminating the need for extensive retraining, making it generally less computationally intensive compared to QAT. PTQ can be categorized into two main categories:
 - *Static quantization* [3, 14, 30, 41, 44, 46]: The weights and activations are quantized to lower precision only once, after the model is trained.
 - *Dynamic quantization* [10]: The weights and activations are quantized during runtime based on specific rules.

In this paper, we focus on a dynamic PTQ technique, specifically LLM.int8() [10]. One of the key innovations in LLM.int8() is identifying and handling outlier feature values that are significantly different from the rest of the values; in contrast, most other quantization methods fail to handle these outliers effectively, leading to a degradation in performance. LLM.int8() addresses this by separating outliers and handling them differently (*i.e.*, their values remain at higher precision) than other feature values.

3. Method

3.1. Preliminaries

As noted in Section 2, in this paper, we focus on the PTQ technique, LLM.int8() [10]. We consider a quantized model $f : \mathcal{X} \rightarrow \mathbb{R}^M$ that receives an input sample $x \in \mathcal{X}$ and outputs M real-valued numbers that represent the model’s confidence for each class $m \in M$, and contains L quantized layers. During inference, for every quantized layer, given the hidden states $\mathbf{X}_{f16} \in \mathbb{R}^{s \times h}$ and weights $\mathbf{W}_{f16} \in \mathbb{R}^{h \times o}$ with sequence dimension s , feature dimension h , and output dimension o , the main steps for efficient matrix multiplication are as follows:

1. **Outlier Extraction:** From the input hidden states \mathbf{X}_{f16} , extract all column indices that contain at least one outlier

Algorithm 1 LLM.int8() Matrix Multiplication

Require: Inputs $X_{f16} \in \mathbb{R}^{s \times h}$, Weights $W_{f16} \in \mathbb{R}^{h \times o}$, Threshold $\tau \in \mathbb{R}$

- 1: $O \leftarrow \emptyset$ {Initialize outlier set}
- 2: **for** $i \leftarrow 0$ **to** $h - 1$ **do**
- 3: **if** $\max(X_{f16}[:, i]) > \tau$ **then**
- 4: $O \leftarrow O \cup \{i\}$ {Add index to outliers}
- 5: **end if**
- 6: **end for**
- 7: $X_{i8} \leftarrow \text{quantize}(X_{f16})$ {Quantize input}
- 8: $W_{i8} \leftarrow \text{quantize}(W_{f16})$ {Quantize weights}
- 9: $M_{out} \leftarrow \text{matmul_f16}(X_{f16}[O], W_{f16}[O])$ {f16 multiply for outliers}
- 10: $M_{non} \leftarrow \text{matmul_int8}(X_{i8}, W_{i8}[\bar{O}])$ {Int8 multiply for non-outliers}
- 11: $M_{non} \leftarrow \text{dequantize}(M_{non})$ {Dequantize result}
- 12: $C_{f16} \leftarrow M_{out} + M_{non}$ {Combine results}
- 13: **return** C_{f16}

- (*i.e.*, values that are larger than a certain threshold τ) into the set $O = \{i | \exists \mathbf{X}_{f16}^i > \tau, 0 \leq i \leq h\}$.
2. **Mixed-Precision Multiplication:** The matrix multiplication process is divided into two segments. Outliers are multiplied using the standard matrix multiplication in float16, while non-outliers are first quantized to their 8-bit representation and then multiplied in int8. This involves row-wise quantization for the hidden state and column-wise quantization for the weight matrix.
 3. **Dequantization and Aggregation:** The non-outlier results are dequantized back to float16 and combined with the outlier results to form the final output.

More formally, the matrix multiplication can be described as:

$$\mathbf{C}_{f16} \approx \sum_{h \in O} \mathbf{X}_{f16}^h \mathbf{W}_{f16}^h + \mathbf{S}_{f16} \cdot \sum_{h \notin O} \mathbf{X}_{i8}^h \mathbf{W}_{i8}^h \quad (1)$$

where C_{f16} represents the output tensor in float16, (X_{f16}^h, W_{f16}^h) represent the float16 input and weight for outliers, S_{f16} is the denormalization term for int8 inputs and weights, and (X_{i8}^h, W_{i8}^h) represent the int8 input and weight for non-outliers. The full procedure is shown in Algorithm 1.

Additional details on quantization and de-quantization can be found in the supplementary material.

3.2. Threat Model

Adversary’s Goals. We consider an adversary whose primary goal is to generate an adversarial perturbation δ that triggers the worst-case performance of dynamic quantization techniques, *i.e.*, increases the number of high-bit operations. Along with our primary goal, to increase the stealth-

ness of the attack, we aim to: (a) maintain the original classification, and (b) generate a smooth perturbation.

Adversary’s Knowledge. To assess the security vulnerability of dynamic quantization to adversarial attacks, we consider two scenarios: (i) a white-box scenario: the attacker has full knowledge about the victim model, and (ii) a black-box scenario: the attacker crafts a perturbation on a surrogate model and applies it to a different victim model.

Attack Variants. Given a dataset \mathcal{D} that contains multiple pairs (x_i, y_i) where x_i is a sample and y_i is the corresponding label, we consider three variants: (i) single - a different perturbation δ is crafted for each $x \in \mathcal{D}$; (ii) class-universal - a single perturbation δ is crafted for a target class $m \in M$; and (iii) universal - a single perturbation δ is crafted for all $x \in \mathcal{D}$.

3.3. The Quant Attack

To achieve the goals presented above, we utilize the PGD attack [26] with a modified loss function. The update of the perturbation δ in iteration t is formulated as follows:

$$\delta^{t+1} = \prod_{\|\delta\|_p < \epsilon} (\delta^t + \alpha \cdot \text{sgn}(\nabla_{\delta} \sum_{(x,y) \in \mathcal{D}'} \mathcal{L}(x,y))) \quad (2)$$

where α is the step size, \prod is the projection operator that enforces $\|\delta\|_p < \epsilon$ for some norm p , and \mathcal{L} is the loss function. The selection of \mathcal{D}' depends on the attack variant: (i) for the single-image variant, $\mathcal{D}' = \{(x,y)\}$; (ii) for the class-universal variant with a target class $m \in M$, $\mathcal{D}' = \{(x,y) \in \mathcal{D} | y = m\}$; and (iii) for the universal variant, $\mathcal{D}' = \mathcal{D}$. Next, we describe the proposed custom loss function, which consists of three components:

$$\mathcal{L} = \lambda_1 \cdot \mathcal{L}_{\text{quant}} + \lambda_2 \cdot \mathcal{L}_{\text{acc}} + \lambda_3 \cdot \mathcal{L}_{\text{TV}} \quad (3)$$

where λ_1, λ_2 , and λ_3 are empirically determined using the grid search approach. The three components are described below.

Quantization Loss. This component aims to achieve our main goal, increasing the number of multiplications in 16-bit precision. The number of multiplications in a higher precision level depends on the existence of an outlier value in each column in the input hidden state matrix. Therefore, practically, we aim to produce at least one “synthetic” outlier value in each column in the input matrix.

Formally, let $\mathbf{X}_l \in \mathbb{R}^{s \times h}$ denote the input hidden state of the l^{th} quantized layer (we omit the bit-precision notation for simplicity). For each input matrix \mathbf{X}_l , we extract the top- K values, denoted as $\mathbf{X}_l^{\text{top-k}} \in \mathbb{R}^{K \times h}$, with the aim of pushing these values towards a target value x_{target} , such that $x_{\text{target}} > \tau$. The loss component for a single layer is defined as follows:

$$\mathcal{L}_{\text{single-quant}}(\mathbf{X}_l^{\text{top-k}}) = \frac{1}{K \cdot h} \sum_{i,j} \max(\mathbf{X}_l^{\text{top-k}}(i,j) - x_{\text{target}}, 0)^2 \quad (4)$$

where (i, j) denote the value in the i^{th} column and j^{th} row. We use $\max(\cdot, 0)$ to make sure that outlier values that already exist are not penalized by the loss function. Finally, the loss for all L layers is defined as:

$$\mathcal{L}_{\text{quant}} = \sum_l^L \mathcal{L}_{\text{single-quant}}(\mathbf{X}_l^{\text{top-k}}) \quad (5)$$

Classification Loss. To increase the stealthiness of our attack, we aim to preserve the original classification of the input image. Therefore, we include the classification loss component, which is defined as follows:

$$\mathcal{L}_{\text{acc}} = \frac{1}{M} \sum_{m=1}^M (f_m(x + \delta) - f_m(x))^2 \quad (6)$$

where f_m denotes the score for class m .

Total Variation (TV) Loss. Since we focus on vision transformers, which split the input image into a sequence of fixed-size 2D patches, the resulting adversarial perturbation contains heavy contours of these patches. To eliminate this, we include the total variation loss which enforces smooth color transitions between neighboring pixels and is defined as follows:

$$\mathcal{L}_{\text{TV}} = \sum_{i,j} \sqrt{(\delta_{i+1,j} - \delta_{i,j})^2 + (\delta_{i,j+1} - \delta_{i,j})^2} \quad (7)$$

where $\delta_{i,j}$ denotes the pixel value at location (i, j) .

4. Evaluation

4.1. Evaluation Setup

4.1.1 Models

We evaluated our attack on two state-of-the-art vision transformers, provided by the Hugging Face framework [11]:

- **Vision Transformer (ViT) [12]:** We use the *base* size version, pretrained on ImageNet-21K (14 million images, 21,843 classes), at a resolution of 224x224. The model is then finetuned on ImageNet-1K (1 million images, 1000 classes). Images are presented to the model as a sequence of fixed-size patches (resolution 16x16).
- **Data-efficient image Transformer (DeiT) [39]:** We use the *base* size version, pretrained and finetuned on ImageNet-1K (1 million images, 1000 classes), at a resolution of 224x224. Images are presented to the model as a sequence of fixed-size patches (resolution 16x16).

Since the quantization technique used in this paper was originally proposed for the NLP domain, we first verified the performance on the quantized models. We compare the accuracy performance of the quantized and non-quantized models across 5,000 images randomly selected from the ImageNet-1K dataset’s validation set. The results show

	Loss Component			ViT	DeiT
	Quantization	Classification	TV	Time / Memory / Energy / Accuracy / Outliers	
Stage 1	✓			11.79% / 29.03% / 6.52% / 22% / 2425.22%	11.13% / 32.35% / 6.55% / 4% / 488.77%
Stage 2	✓	✓		11.26% / 27.43% / 6.74% / 93% / 2278.20%	11.06% / 31.89% / 6.46% / 92% / 486.28%
Stage 3	✓	✓	✓	10.90% / 23.06% / 7.01% / 94% / 2180.83%	10.25% / 26.80% / 5.85% / 93% / 453.50%

Table 1. Comparative analysis of ViT and DeiT models for different loss function components. The values (except accuracy) represent the percentage change between the perturbed and original images.

that the quantized model exhibits the same level of performance as the non-quantized model. For ViT, the accuracy is 80.51% and 80.59% for the quantized and non-quantized models, respectively. For DeiT, the accuracy is 80.47% and 80.57% for the quantized and non-quantized models, respectively. This demonstrates that the LLM.int8() technique is applicable for the vision domain.

4.1.2 Datasets

In our evaluation, we use the ImageNet dataset [9], and specifically, the images from its validation set, which were not used to train the models described above. For the single-image attack variant, we trained and tested our attack on 500 random images from various class categories. For the class-universal variant, we selected 10 random classes, and for each class we trained the perturbation on 250 images (*i.e.*, $|\mathcal{D}| = 250$) and tested them on a distinct set of 500 images from the same class. Similarly, for the universal variant, we followed the same training and testing procedure, however from different class categories.

4.1.3 Metrics

To evaluate the effectiveness of our attack, we examine the number of outlier multiplications, different hardware metrics, and the effect of the attack on the model’s original task performance:

- **GPU Memory Consumption:** how much GPU memory the process uses.
- **GPU Response Time:** how long the GPU takes to perform calculations.
- **Energy Consumption:** the total energy usage of the GPU, with measurements obtained using the NVIDIA Management Library (NVML).
- **Number of Outliers:** represents the number of matrix multiplications done in 16-bit precision (see Section 2).
- **Accuracy:** the performance of the model on its original task. We consider the model’s prediction on the original images as the ground-truth label.

4.1.4 Implementation Details

In our attack, we focus on ℓ_{inf} norm bounded perturbations, and set $\epsilon = 0.8$. We use a cosine annealing strategy with warm restarts for the attack’s step size α , where the

maximum and minimum values are 0.02 and $10e - 6$, respectively. For the dynamic quantization threshold, we set $\tau = 6$, as suggested in the original paper [10]. We set the target value of our attack x_{target} to 70 and the number of extracted values from each column k to 4, as they empirically yielded the best results. The results of the ablation studies we performed on the ϵ , k , and x_{target} values can be found in the supplementary material. The experiments are conducted on a GeForce RTX 3090 GPU. To stabilize the performance metrics, we execute a GPU warm-up routine twice before starting to record the performance.

4.2. Results

4.2.1 Effect of the Loss Components

We first investigate the effect of the additional loss components presented in Section 3.3, classification and TV loss. Specifically, we examine each component’s contribution to the goal it was designed to achieve: (i) classification loss \mathcal{L}_{acc} - preserve the classification original, and (ii) TV loss \mathcal{L}_{TV} - smooth color transitions between neighboring pixels. To this end, we experiment with three different settings: quantization loss only ($(\lambda_2, \lambda_3) = (0, 0)$), quantization loss with classification loss ($\lambda_3 = 0$), and a combination of the three components. Table 1 presents the results for the various combinations on the ViT and DeiT models. As can be seen, when the classification loss is included in the loss (Stage 2 and Stage 3), the accuracy substantially improves compared to the baseline (*e.g.*, the average accuracy on the DeiT model increases from 4% to 92%). Since the TV loss component’s contribution is not quantifiable, we only verify that it does not negatively affect the performance of the attack and classification (Stage 3). Figure 1 provides a visual example of the attack with and without the TV component. As can be seen in Figure 1b, since our attack is performed on vision transformers which split the image into fixed-size patches, the perturbation heavily emphasizes these splits, resulting in a less stealthy attack. In Figure 1c, we show that the inclusion of the TV component smooths the color transitions between the different patches. The combination of all the components results in an imperceptible perturbation that is not only resource-exhaustive but also possesses the predictive capability. In the remainder of this section, the results presented were obtained using the following configuration for the loss function: $(\lambda_1, \lambda_2, \lambda_3) = (1, 0.01, 50)$.

Perturbation Type	ViT					DeiT				
	GPU Mem [Mbits]	Energy [mJ]	GPU Time [ms]	Accuracy	Outliers	GPU Mem [Mbits]	Energy [mJ]	GPU Time [ms]	Accuracy	Outliers
Clean	707.78	331908.49	20.19	1.00	236	865.65	497946.28	27.91	1.00	1516.42
	1.00×	1.00×	1.00×	-	1.00×	1.00×	1.00×	1.00×	-	1.00×
Random	706.69	324425.70	19.95	0.21	234.73	869.44	499843.03	27.99	0.62	1566.05
	0.99×	0.97×	0.98×	-	0.99×	1.003×	1.003×	1.003×	-	1.03×
Universal	778.66	345517.30	21.2	0.29	2400.19	969.44	503888.90	30.15	0.17	7023.23
	1.10×	1.04×	1.05×	-	10.16×	1.12×	1.012×	1.08×	-	4.63×
Class-Universal	789.45	346586.70	21.30	0.86	2481.78	985.8	508566.3	30.29	0.74	7413.45
	1.11×	1.045×	1.067×	-	10.51×	1.14×	1.021×	1.085×	-	4.89×
Single	871.04	355239.33	22.42	0.94	5402.00	1097.19	527078.59	30.77	0.93	8668.88
	1.23×	1.07×	1.11×	-	22.88×	1.26×	1.06×	1.10×	-	5.53×

Table 2. Evaluation of ViT and DeiT models on different baselines and attack variations. The bottom number represents the percentage change from the clean image performance. Bold indicates superior results.

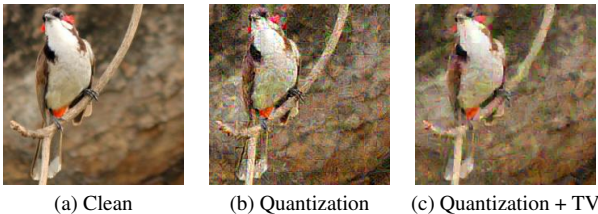


Figure 1. An example of (a) a clean image; (b) a perturbed image attacked with the quantization loss component only; and (c) a perturbed image attacked with both the quantization and TV loss components (Best viewed in color, zoomed-in).

The complete results, including the results of the grid search performed on the λ hyperparameters, can be found in the supplementary material.

4.2.2 Effectiveness of Adversarial Perturbations

First, we evaluate the effectiveness of our single-image variant against two baselines: a clean image (*i.e.*, no perturbation) and a random perturbation sampled from the uniform distribution $\mathcal{U}(-1, 1)$ (the values correspond to the minimum and maximum values of our perturbation for a fair comparison). Table 2 presents the performance of the different perturbations on the ViT and DeiT models. The analysis reveals that single-image perturbations substantially increase the GPU memory usage and processing time for both models compared to the baselines. Specifically, for the ViT model, the single-image perturbations cause 2288% more outliers than a clean image. In terms of hardware metrics, they result in a 23% increase in GPU memory usage, a 7% increase in energy consumption, and an 11% increase in GPU processing time, compared to clean images. Interestingly, in most cases, the random perturbations lead to a degradation in performance compared to the clean images. We hypothesize that random perturbations simply eliminate “natural” outlier features (*i.e.*, those that exist in clean images) due to the random noise added to the images.

4.2.3 Universal and Class-Universal Perturbations

We also investigate the effect of reusable perturbations, in which class-universal and universal perturbations (Section 3.2) are trained on one set of images and tested on a distinct holdout set. The results presented in Table 2 enable comparison of the perturbations’ impact based on various metrics. On the ViT model, when compared to clean images, a universal perturbation results in a 10% increase in GPU memory usage, 4% increase in energy consumption, and 5% increase in GPU processing time. Class-specific perturbations cause an 11% increase in GPU memory usage, 4.5% increase in energy consumption, and 6.7% increase in GPU time, performing slightly better than the universal perturbation.

Although universal and class-specific perturbations are less resource-exhaustive than single-image perturbations, they offer a distinct advantage. A universal perturbation vector is capable of affecting multiple images or an entire class of images, thereby providing an efficient mechanism for broad-spectrum adversarial attacks. This efficiency is especially advantageous in scenarios where the attacker aims to disrupt the model across multiple data points with minimal computational effort.

When examining the effect of these perturbations, we observed an interesting phenomena: When we relax the assumption that the perturbation must be imperceptible (*i.e.*, the noise bound ϵ is set at a high value), the resulting perturbation obliterates the visual appearance of the input image entirely, visually resembling sheer noise. This results in a resource-intensive scenario which could be interpreted as a denial-of-service (DoS) attack. By relaxing the assumption in this way, we were able to increase GPU memory usage by 70%, energy consumption by 12%, and GPU time by 25%.

4.2.4 Batch Attack

In the LLM.int8() [10] technique, when the quantized model processes a batch of B images, every quantized layer transforms the given 3D input matrix $\mathbf{X}_{f16} \in \mathbb{R}^{B \times s \times h}$ to a stacked 2D version $\mathbf{X}_{f16} \in \mathbb{R}^{(B \cdot s) \times h}$, resulting in $B \times$

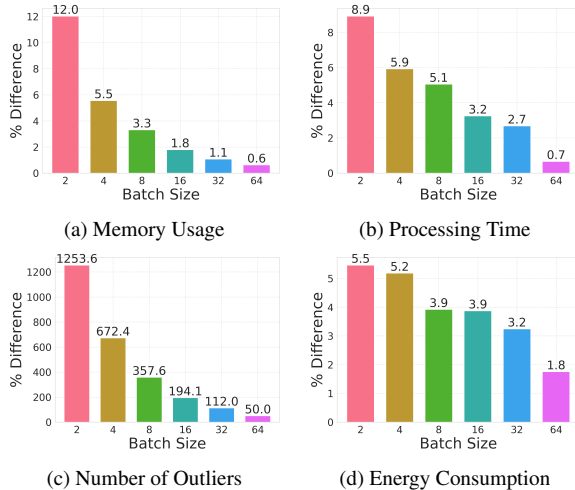


Figure 2. Evaluating the influence of a single perturbed image in a batch for different batch sizes. The values represent the percentage difference between a benign batch and its attacked counterpart.

more rows. The transformation is followed by quantized matrix multiplication (Section 3). In this case, when an outlier value exists in a column, the entire column is processed in f16 precision, including values in rows that belong to a completely different image.

In a realistic scenario where a quantized model is deployed and serves as ML-as-a-service, input images from different sources can be stacked together and given to the model as a batch of images. In this case, an adversary could potentially implant a perturbed image that will affect the resource consumption of the whole batch.

Therefore, we evaluate the impact of such a scenario in which we feed the quantized model different sized batches that include a single perturbed image. Figure 2 presents the results for the different batch sizes; the values represent the percentage difference between a benign batch and its attacked counterpart. The results show that a perturbed image implanted in a batch of images could potentially affect the performance of the entire batch, as an increase in resource consumption is seen for all of the batch sizes examined. Notably, smaller size batches (*e.g.*, two images) are more sensitive than larger size batches (*e.g.*, 16 images). For example, for a two-image batch, the memory usage increases by 12% compared to the benign batch, while for a 16-image batch, the memory only increases by 1.8%. A plausible explanation for this can be found in the initial state of the batches - with a large batch size, natural outliers from different images are likely to spread across multiple columns. Consequently, the attacked image could contain synthetic outliers in the same columns, which are already processed in float16, and this leads to a smaller percentage difference.

	Single Model		Ensemble	
	Train: DeiT Test: ViT	Train: ViT Test: DeiT	Train: DeiT+ViT Test: ViT	Train: DeiT+ViT Test: DeiT
GPU mem	0.2%	2.5%	18.83%	26.91%
GPU time	-1.00%	0%	9.06%	10.01%
Outliers	22.84%	19%	1616.5%	431.73%

Table 3. Transferability and ensemble analysis. Values indicate the percentage difference between perturbed and clean images.

4.2.5 Transferability and Ensemble Approaches

In adversarial attacks, transferability refers to the ability of an adversarial example, crafted on a surrogate model, to affect other models. In our experiments, we examine the effect of perturbations trained on ViT and tested on DeiT and vice versa. As shown in Table 3, adversarial examples trained on one model show limited impact on the other. Interestingly, we observed an unexpected anomaly in the GPU time when perturbations were trained on DeiT and tested on ViT, in which a negative value was recorded (*i.e.*, the GPU time decreased). We hypothesize that this occurred due to the marginal effect of just 22.84% more outliers. Such anomalies emphasize the nuanced relationship between outliers and resource metrics, hinting at the complex performance environment within which these models operate. Despite this minor deviation, the general trend remains consistent: a higher number of outliers usually requires more resources.

To improve the transferability between different models, we employ an ensemble training strategy, in which the adversarial example is trained on both models simultaneously, such that in each training iteration one of the models is randomly selected. This approach aims to examine the collaborative benefit of utilizing the strengths of both models to create generalizable adversarial perturbations. Based on the results presented in Table 3, we can see that the ensemble strategy is able to affect both models, and results in an increase in GPU memory usage and GPU time, although with slightly less efficiency compared to perturbations trained and tested on the same model. For example, when the ensemble-based perturbations are tested on the DeiT model, GPU memory usage and GPU time increased by 26.91% and 10.01%, respectively.

4.2.6 Evaluating Across Diverse Model Architectures

To emphasize the potential impact and generalizability of our attack, we also experiment with other models that have different characteristics: different computer vision tasks, and different modalities. In addition, we also broaden our analysis from the computer vision domain to include the audio domain. It should be noted that in our attack against those models, we only use the single-image attack variant with the quantization loss component (*i.e.*, $(\lambda_2, \lambda_3) =$

Model	GPU Mem [Mbits]		Energy [mJ]		GPU Time [ms]		Outliers	
	Clean	Single	Clean	Single	Clean	Single	Clean	Single
OWLv2 [27]	24691.10	26821.05	1242041.43	1297153.75	193.97	220.47	8375.75	44652.68
	1.00×	1.086×	1.00×	1.045×	1.00×	1.137×	1.00×	5.337×
YOLOS [15]	13441.00	13771.35	552024.84	632745.58	161.21	168.15	388.09	7400.86
	1.00×	1.025×	1.00×	1.148×	1.00×	1.043×	1.00×	19.876×
GIT [40]	4593.50	4758.20	768206.85	803760.53	252.90	254.61	3405.70	7072.02
	1.00×	1.03×	1.00×	1.046×	1.00×	1.006×	1.00×	2.07×
Whisper [33]	1314.88	1444.89	214687.04	222644.96	18.90	20.44	1647.71	6519.76
	1.00×	1.09×	1.00×	1.03×	1.00×	1.08×	1.00×	3.95×

Table 4. Comprehensive evaluation of the performance of QuantAttack (single-image variant) on various computer vision and audio models. The bottom number represents the percentage change from the clean image performance.

(0, 0)) for simplicity. We also note that the same attack configuration used for the image classification models (Section 4.1.4) is used for all the evaluated models below, which might lead to suboptimal results.

Open-World Localization (OWLv2) [27] is a zero-shot text-conditioned object detection model that combines visual and text features using a CLIP backbone [32], efficiently performing open-vocabulary object detection. In our evaluation, we use 500 images from the COCO dataset [24], and the corresponding texts are simply the concatenation of the class categories in each image. As shown in Table 4, the perturbations successfully compromise the GPU availability, increasing the GPU time by 13.7% compared to the clean images.

You Only Look at One Sequence (YOLOS) [15] is a transformer-based object detection model. It employs a bipartite matching loss and the Hungarian algorithm, resulting in a simplified yet effective approach for object detection tasks. The results, presented in Table 4, show an interesting phenomena. While our attack is able to increase the number of outliers by 1987% (the largest increase across all models), a substantial effect is only seen in energy consumption where there is a 14.8% increase. In this case, the increase in memory usage and GPU time is not correlated to the number of outliers, leading to a 2.5% and 4.3% increase, respectively.

Generative Image-to-text Transformer (GIT) [40] is a decoder-only transformer for vision-language tasks that utilizes CLIP’s vision encoder for integrated text and image processing. During our evaluation, we focus on its image captioning abilities, in which an image is provided as input and the model is asked generate a corresponding caption. The results presented in Table 4 show that our attack does not affect GIT as much as it affects the other models, where a 4.5% increase in the energy consumption is seen.

Whisper [33] is a sequence-to-sequence model for automatic speech recognition (ASR) and speech translation. Since Whisper is fully differentiable, similar to the computer vision models above, it is also vulnerable to adversar-

ial perturbations that tamper with the input audio by adding an imperceptible, carefully-crafted pattern. To demonstrate that our attack also extends to the audio domain, we employ a technique similar to the one employed for the computer vision models, in order to generate the adversarial examples. We use 500 utterances from the FLEURS dataset [8] and examine our attack’s effect on a quantized Whisper model. As shown in Table 4, Whisper exhibits a noticeable increase in resource consumption. The GPU memory usage increases by 9%, energy consumption increases by 3%, and GPU time increases by 8.1%.

5. Countermeasures

In response to the challenges posed by QuantAttack, in this section, we propose two practical steps that can be performed to enhance the security of the quantization process: **Limiting the use of high-precision multiplications** – implement rules that limit when and how often the model uses high-precision calculations. This approach, however, may negatively affect the quantization performance, failing to capture all natural outliers, which has been shown to be the cause of performance degradation in static quantization techniques [10]. **Increasing the batch size** – based on our observations (Figure 2), increasing the batch size reduces QuantAttack’s impact due to a higher occurrence of natural outliers. In this case, the synthetic outliers that our attack produces might blend with the natural outliers (*i.e.*, the number of high-precision multiplications will not increase linearly). Nonetheless, the quantization’s efficiency decreases as the batch size grows. Above all, both approaches have trade-offs between performance and security, demonstrating that there is no perfect solution that will completely eliminate the threat posed by our attack.

6. Conclusion

In this paper, we presented QuantAttack, a novel adversarial attack that both exploits the vulnerabilities and highlights the risk of using vision transformers with dynamic quantization. We showed that quantized models, while bene-

fitting from the quantization’s efficiency, are susceptible to availability-oriented adversarial techniques that can degrade their performance. Our comprehensive evaluation demonstrated the impact of our attack on a wide range of vision transformers in various attack configurations. The implications of these findings are significant, indicating the pressing need to develop more robust quantization methods that can withstand such adversarial challenges. In future work, we plan to explore the applicability of our attack in the NLP domain and evaluate its impact on popular large language models (LLMs).

References

- [1] Vahid Behzadan and William Hsu. Adversarial exploitation of policy imitation. *arXiv preprint arXiv:1906.01121*, 2019. [2](#)
- [2] Yash Bhalgat, Jinwon Lee, Markus Nagel, Tijmen Blankevoort, and Nojun Kwak. Lsq+: Improving low-bit quantization through learnable offsets and better initialization. In *Proceedings of the IEEE/CVF Conference on Computer Vision and Pattern Recognition Workshops*, pages 696–697, 2020. [1](#), [3](#)
- [3] Yelysei Bondarenko, Markus Nagel, and Tijmen Blankevoort. Understanding and overcoming the challenges of efficient transformer quantization. *arXiv preprint arXiv:2109.12948*, 2021. [3](#)
- [4] Nicholas Boucher, Ilia Shumailov, Ross Anderson, and Nicolas Papernot. Bad characters: Imperceptible nlp attacks. In *2022 IEEE Symposium on Security and Privacy (SP)*, pages 1987–2004. IEEE, 2022. [2](#)
- [5] Andrew Boutros, Mathew Hall, Nicolas Papernot, and Vaughn Betz. Neighbors from hell: Voltage attacks against deep learning accelerators on multi-tenant fpgas. In *2020 International Conference on Field-Programmable Technology (ICFPT)*, pages 103–111. IEEE, 2020. [2](#)
- [6] Antonio Emanuele Cinà, Ambra Demontis, Battista Biggio, Fabio Roli, and Marcello Pelillo. Energy-latency attacks via sponge poisoning. *arXiv preprint arXiv:2203.08147*, 2022. [1](#)
- [7] Antonio Emanuele Cinà, Ambra Demontis, Battista Biggio, Fabio Roli, and Marcello Pelillo. Energy-latency attacks via sponge poisoning. *arXiv preprint arXiv:2203.08147*, 2022. [2](#)
- [8] Alexis Conneau, Min Ma, Simran Khanuja, Yu Zhang, Vera Axelrod, Siddharth Dalmia, Jason Riesa, Clara Rivera, and Ankur Bapna. Fleurs: Few-shot learning evaluation of universal representations of speech. In *2022 IEEE Spoken Language Technology Workshop (SLT)*, pages 798–805. IEEE, 2023. [8](#)
- [9] Jia Deng, Wei Dong, Richard Socher, Li-Jia Li, Kai Li, and Li Fei-Fei. Imagenet: A large-scale hierarchical image database. In *2009 IEEE conference on computer vision and pattern recognition*, pages 248–255. Ieee, 2009. [5](#)
- [10] Tim Dettmers, Mike Lewis, Younes Belkada, and Luke Zettlemoyer. Llm.int8(): 8-bit matrix multiplication for transformers at scale. *arXiv preprint arXiv:2208.07339*, 2022. [1](#), [3](#), [5](#), [6](#), [8](#)
- [11] Tim Dettmers, Mike Lewis, Younes Belkada, and Luke Zettlemoyer. A gentle summary of llm.int8(): zero degradation matrix multiplication for large language models, 2022. [4](#)
- [12] Alexey Dosovitskiy, Lucas Beyer, Alexander Kolesnikov, Dirk Weissenborn, Xiaohua Zhai, Thomas Unterthiner, Mostafa Dehghani, Matthias Minderer, Georg Heigold, Sylvain Gelly, et al. An image is worth 16x16 words: Transformers for image recognition at scale. *arXiv preprint arXiv:2010.11929*, 2020. [2](#), [4](#)
- [13] Steven K Esser, Jeffrey L McKinstry, Deepika Bablani, Rathinakumar Appuswamy, and Dharmendra S Modha. Learned step size quantization. *arXiv preprint arXiv:1902.08153*, 2019. [1](#), [3](#)
- [14] Jun Fang, Ali Shafiee, Hamzah Abdel-Aziz, David Thorsley, Georgios Georgiadis, and Joseph H Hassoun. Post-training piecewise linear quantization for deep neural networks. In *Computer Vision–ECCV 2020: 16th European Conference, Glasgow, UK, August 23–28, 2020, Proceedings, Part II 16*, pages 69–86. Springer, 2020. [1](#), [3](#)
- [15] Yuxin Fang, Bencheng Liao, Xinggang Wang, Jiemin Fang, Jiyang Qi, Rui Wu, Jianwei Niu, and Wenyu Liu. You only look at one sequence: Rethinking transformer in vision through object detection. *Advances in Neural Information Processing Systems*, 34:26183–26197, 2021. [8](#)
- [16] Ian J Goodfellow, Jonathon Shlens, and Christian Szegedy. Explaining and harnessing adversarial examples. *arXiv preprint arXiv:1412.6572*, 2014. [2](#)
- [17] Yizeng Han, Gao Huang, Shiji Song, Le Yang, Honghui Wang, and Yulin Wang. Dynamic neural networks: A survey. *IEEE Transactions on Pattern Analysis and Machine Intelligence*, 44(11):7436–7456, 2021. [1](#), [2](#)
- [18] Mirazul Haque, Anki Chauhan, Cong Liu, and Wei Yang. Ilfo: Adversarial attack on adaptive neural networks. In *Proceedings of the IEEE/CVF Conference on Computer Vision and Pattern Recognition*, pages 14264–14273, 2020. [2](#)
- [19] Sanghyun Hong, Yiğitcan Kaya, Ionuț-Vlad Modoranu, and Tudor Dumitraș. A panda? no, it’s a sloth: Slowdown attacks on adaptive multi-exit neural network inference. *arXiv preprint arXiv:2010.02432*, 2020. [2](#)
- [20] Raphaël Joud, Pierre-Alain Moëllic, Rémi Bernhard, and Jean-Baptiste Rigaud. A review of confidentiality threats against embedded neural network models. In *2021 IEEE 7th World Forum on Internet of Things (WF-IoT)*, pages 610–615. IEEE, 2021. [2](#)
- [21] Katikapalli Subramanyam Kalyan, Ajit Rajasekharan, and Sivanesan Sangeetha. Ammus: A survey of transformer-based pretrained models in natural language processing. *arXiv preprint arXiv:2108.05542*, 2021. [1](#)
- [22] Salman Khan, Muzammal Naseer, Munawar Hayat, Syed Waqas Zamir, Fahad Shahbaz Khan, and Mubarak Shah. Transformers in vision: A survey. *ACM computing surveys (CSUR)*, 54(10s):1–41, 2022. [1](#), [2](#)
- [23] Tianyang Lin, Yuxin Wang, Xiangyang Liu, and Xipeng Qiu. A survey of transformers. *AI Open*, 2022. [1](#)

- [24] Tsung-Yi Lin, Michael Maire, Serge Belongie, James Hays, Pietro Perona, Deva Ramanan, Piotr Dollár, and C Lawrence Zitnick. Microsoft coco: Common objects in context. In *Computer Vision—ECCV 2014: 13th European Conference, Zurich, Switzerland, September 6–12, 2014, Proceedings, Part V 13*, pages 740–755. Springer, 2014. 8
- [25] Han Liu, Yuhao Wu, Zhiyuan Yu, Yevgeniy Vorobeychik, and Ning Zhang. Slowlidar: Increasing the latency of lidar-based detection using adversarial examples. In *Proceedings of the IEEE/CVF Conference on Computer Vision and Pattern Recognition*, pages 5146–5155, 2023. 2
- [26] Aleksander Madry, Aleksandar Makelov, Ludwig Schmidt, Dimitris Tsipras, and Adrian Vladu. Towards deep learning models resistant to adversarial attacks. *arXiv preprint arXiv:1706.06083*, 2017. 2, 4
- [27] Matthias Minderer, Alexey Gritsenko, and Neil Houlsby. Scaling open-vocabulary object detection. *arXiv preprint arXiv:2306.09683*, 2023. 8
- [28] Seyed-Mohsen Moosavi-Dezfooli, Alhussein Fawzi, and Pascal Frossard. Deepfool: a simple and accurate method to fool deep neural networks. In *Proceedings of the IEEE conference on computer vision and pattern recognition*, pages 2574–2582, 2016. 2
- [29] Seyed-Mohsen Moosavi-Dezfooli, Alhussein Fawzi, Omar Fawzi, and Pascal Frossard. Universal adversarial perturbations. In *Proceedings of the IEEE conference on computer vision and pattern recognition*, pages 1765–1773, 2017. 2
- [30] Markus Nagel, Rana Ali Amjad, Mart Van Baalen, Christos Louizos, and Tijmen Blankevoort. Up or down? adaptive rounding for post-training quantization. In *International Conference on Machine Learning*, pages 7197–7206. PMLR, 2020. 1, 3
- [31] Jianhong Pan, Qichen Zheng, Zhipeng Fan, Hossein Rahmani, Qihong Ke, and Jun Liu. Gradauto: Energy-oriented attack on dynamic neural networks. In *European Conference on Computer Vision*, pages 637–653. Springer, 2022. 2
- [32] Alec Radford, Jong Wook Kim, Chris Hallacy, Aditya Ramesh, Gabriel Goh, Sandhini Agarwal, Girish Sastry, Amanda Askell, Pamela Mishkin, Jack Clark, et al. Learning transferable visual models from natural language supervision. In *International conference on machine learning*, pages 8748–8763. PMLR, 2021. 8
- [33] Alec Radford, Jong Wook Kim, Tao Xu, Greg Brockman, Christine McLeavey, and Ilya Sutskever. Robust speech recognition via large-scale weak supervision. In *International Conference on Machine Learning*, pages 28492–28518. PMLR, 2023. 8
- [34] Spyridon Samonas and David Coss. The cia strikes back: Redefining confidentiality, integrity and availability in security. *Journal of Information System Security*, 10(3), 2014. 2
- [35] Avishag Shapira, Alon Zolfi, Luca Demetrio, Battista Biggio, and Asaf Shabtai. Phantom sponges: Exploiting non-maximum suppression to attack deep object detectors. In *Proceedings of the IEEE/CVF Winter Conference on Applications of Computer Vision*, pages 4571–4580, 2023. 2
- [36] Ilia Shumailov, Yiren Zhao, Daniel Bates, Nicolas Papernot, Robert Mullins, and Ross Anderson. Sponge examples: Energy-latency attacks on neural networks. In *2021 IEEE European symposium on security and privacy (EuroS&P)*, pages 212–231. IEEE, 2021. 1, 2
- [37] Chawin Sitawarin, Arjun Nitin Bhagoji, Arsalan Mosenia, Mung Chiang, and Prateek Mittal. Darts: Deceiving autonomous cars with toxic signs. *arXiv preprint arXiv:1802.06430*, 2018. 2
- [38] Christian Szegedy, Wojciech Zaremba, Ilya Sutskever, Joan Bruna, Dumitru Erhan, Ian Goodfellow, and Rob Fergus. Intriguing properties of neural networks. *arXiv preprint arXiv:1312.6199*, 2013. 2
- [39] Hugo Touvron, Matthieu Cord, Matthijs Douze, Francisco Massa, Alexandre Sablayrolles, and Hervé Jégou. Training data-efficient image transformers & distillation through attention. In *International conference on machine learning*, pages 10347–10357. PMLR, 2021. 4
- [40] Jianfeng Wang, Zhengyuan Yang, Xiaowei Hu, Linjie Li, Kevin Lin, Zhe Gan, Zicheng Liu, Ce Liu, and Lijuan Wang. Git: A generative image-to-text transformer for vision and language. *ArXiv*, abs/2103.01260, 2021. 8
- [41] Peisong Wang, Qiang Chen, Xiangyu He, and Jian Cheng. Towards accurate post-training network quantization via bit-split and stitching. In *International Conference on Machine Learning*, pages 9847–9856. PMLR, 2020. 1, 3
- [42] Thomas Wolf, Lysandre Debut, Victor Sanh, Julien Chaumond, Clement Delangue, Anthony Moi, Pierric Cistac, Tim Rault, Rémi Louf, Morgan Funtowicz, et al. Huggingface’s transformers: State-of-the-art natural language processing. *arXiv preprint arXiv:1910.03771*, 2019. 1
- [43] Thomas Wolf, Lysandre Debut, Victor Sanh, Julien Chaumond, Clement Delangue, Anthony Moi, Pierric Cistac, Tim Rault, Rémi Louf, Morgan Funtowicz, et al. Transformers: State-of-the-art natural language processing. In *Proceedings of the 2020 conference on empirical methods in natural language processing: system demonstrations*, pages 38–45, 2020. 2
- [44] Guangxuan Xiao, Ji Lin, Mickael Seznec, Hao Wu, Julien Demouth, and Song Han. Smoothquant: Accurate and efficient post-training quantization for large language models. In *International Conference on Machine Learning*, pages 38087–38099. PMLR, 2023. 3
- [45] Kaidi Xu, Gaoyuan Zhang, Sijia Liu, Quanfu Fan, Mengshu Sun, Hongge Chen, Pin-Yu Chen, Yanzhi Wang, and Xue Lin. Adversarial t-shirt! evading person detectors in a physical world. In *Computer Vision—ECCV 2020: 16th European Conference, Glasgow, UK, August 23–28, 2020, Proceedings, Part V 16*, pages 665–681. Springer, 2020. 2
- [46] Zhewei Yao, Reza Yazdani Aminabadi, Minjia Zhang, Xiaoxia Wu, Conglong Li, and Yuxiong He. Zeroquant: Efficient and affordable post-training quantization for large-scale transformers. *Advances in Neural Information Processing Systems*, 35:27168–27183, 2022. 3
- [47] Shuchang Zhou, Yuxin Wu, Zekun Ni, Xinyu Zhou, He Wen, and Yuheng Zou. Dorefa-net: Training low bitwidth convolutional neural networks with low bitwidth gradients. *arXiv preprint arXiv:1606.06160*, 2016. 1, 3
- [48] Alon Zolfi, Moshe Kravchik, Yuval Elovici, and Asaf Shabtai. The translucent patch: A physical and universal attack

on object detectors. In *Proceedings of the IEEE/CVF Conference on Computer Vision and Pattern Recognition*, pages 15232–15241, 2021. [2](#)

- [49] Alon Zolfi, Shai Avidan, Yuval Elovici, and Asaf Shabtai. Adversarial mask: Real-world universal adversarial attack on face recognition models. In *Joint European Conference on Machine Learning and Knowledge Discovery in Databases*, pages 304–320. Springer, 2022. [2](#)